

# Kinetic theory of spin transport in $n$ -typed semiconductor quantum wells

M. Q. Weng<sup>b</sup> and M. W. Wu<sup>a,b,\*</sup>

<sup>a</sup>Structure Research Laboratory, University of Science & Technology of China, Academia Sinica, Hefei, Anhui, 230026, China

<sup>b</sup>Department of Physics, University of Science & Technology of China, Hefei, Anhui, 230026, China<sup>\*\*</sup>

(February 7, 2020)

We set up a set of many-body kinetic Bloch equations with spacial inhomogeneity. We reexamine the widely adopted quasi-independent electron model (QIEM) and show the inadequacy of this model in studying the spin transport. We further point out a new decoherence effect based on interference effect of electrons/spins with different momentum  $\mathbf{k}$  along the direction of the diffusion, which is referred as “inhomogeneous broadening effect” in our paper. We show that this inhomogeneous broadening can cause spin decoherence alone even in the absence of the scattering and that the resulting decoherence can be more important than the dephasing effect due to the D'yakonov-Perel' (DP) term together with the scattering. Our theory takes all the inhomogeneous broadening effect, the spin diffusion due to the spacial inhomogeneity and the spin dephasing into account and gets the results self-consistently. We further study the spin diffusion/transport of an  $n$ -typed GaAs quantum well (QW) in the steady state under different conditions, such as at different temperatures; in the presence of impurities; in the presence of external electric fields along the diffusion direction and/or the QW growth direction; and with magnetic fields in the Voigt configuration. We also demonstrate a time evolution of a spin package calculated from our many-body theory. Different features predicted from our many-body theory are highlighted in the paper.

PACS: 72.25.Dc; 72.25.Rb; 71.55.Eg; 73.21.Fg

## I. INTRODUCTION

Study of spintronics has attracted tremendous attention in recent years, both in theoretical and experimental circles<sup>1</sup>, thanks to the discovery of the long-lived (sometimes  $> 100$  ns) coherent electron spin states in  $n$ -typed semiconductors<sup>2-7</sup>. Possible applications of spintronics include qubits for quantum computers, quantum memory devices, spin transistors, and spin valves etc. The last two applications involve transporting an electronic spin polarization from a place to another by means of an electrical or diffusive current. Therefore, it is of great importance to study the spin transport. Apart from the great number of works on spin injection, there are only a few experimental reports on spin coherent transport over macroscopic distance<sup>3,8,9</sup>. On theoretical aspect, most works are based on the QIEM and focused on the diffusive transport regime<sup>10-16</sup>, where equations for spin polarized currents can be set up and the longitudinal spin dephasing, generally referred to as spin diffusion length can be achieved. In these theories, the mechanism for the spin relaxation is assumed due to the spin-flipping scattering. Without scattering, the spin polarization will not decay. In Ref. 17, Takahashi *et al.* calculated the scattering induced spin relaxation time associated with the spin diffusion from the many body kinetic equations.

Of particular interest to the spin transport theory in semiconductors has been the question as to whether the QIEM can adequately account for the experimental results or whether many-body process is important. Flatte *et al.* have concluded that an independent electron approach is quite capable of explaining measurements of spin lifetimes in the diffusive regime<sup>18</sup>. In this paper, we

first extend a many-body kinetic theory developed by Wu *et al.* to describe the spin precession and dephasing in insulating sample as well as  $n$ -doped sample<sup>19-21</sup> to the spacial inhomogeneous regime, and get the many-body transport equations to investigate the spin diffusion in  $n$ -doped GaAs quantum QW system. Here, we only focus on the spin transport inside the semiconductors and avoid the problem of spin injection at the boundary. Facilitated with the full many-body transport theory, we are able to reexamine above mentioned issue and show the inadequacy of the independent electron model in describing the spin transport. We also propose a mechanism that may cause strong longitudinal spin decoherence in addition to the spin dephasing due to the scattering. The new mechanism results from the interference effect due to the wavevector dependence along the spacial gradients of the spin densities in the spin diffusion. This wavevector dependence can be considered as some sort of “inhomogeneous broadening”, which can cause spin decay alone, even without the scattering. We further study the spin transport/diffusion under different conditions. The methods developed in this paper can be well applied to the spintronic device modeling.

We organize this paper as follows: We present the model and the full many-body kinetic equations in Sec. II. In Sec. III we first reduce the full kinetic equations obtained in Sec. II to the equations of the single electron approach (*i.e.*, QIEM). We then show how the many-body-interference-induced spin decoherence which is missing in the single electron approach. Then we discuss in detail the solution of the full many-body transport equations for an  $n$ -typed single QW in the steady state in Sec. IV under different conditions: In Sec. IV(A) we study

the spin diffusion without an applied electric field in the absence/presence of impurities. We also investigate the magnetic field and the temperature effect to the spin diffusion in Voigt configuration. Then in Sec IV(B) we show the spin transport with an electric field in the absence/presence of impurities. The contributions due to the Rashba term are given in Sec. IV(C). Differing from the single electron approach where the diffusion length is limited by the dephasing, the diffusion length predicted by our full many-body theory is limited by both dephasing and decoherence effects. In Sec. IV(D) we compare the diffusion length obtained from our full many-body calculation with that of single electron calculation. In Sec. V we show the evolution of spin diffusion of an initial spin polarization. In these studies, we highlight the difference of our many-body theory to the single electron approach. We summarize our main results and conclusions in Sec. VI.

## II. MODEL AND KINETIC EQUATIONS

We start our investigation from an  $n$ -doped (100) GaAs QW with well width  $a$ . The growth direction is assumed to be the  $z$  axis. A moderate magnetic field  $\mathbf{B}$  together with an electric field are applied along the  $x$  axis. Due to the confinement of the QW, the momentum states along  $z$  axis are quantized. Therefore the electron states are characterized by a subband index  $n$  and a two dimensional wave vector  $\mathbf{k} = (k_x, k_y)$ , together with a spin index  $\sigma$ . In the present paper, the subband separation is assumed to be large enough so that only the lowest subband is populated and the transition to the upper subbands is unimportant. Therefore, one only needs to consider the lowest subband. For  $n$ -doped samples, spin dephasing mainly comes from the DP mechanism<sup>22</sup>. With the DP term included, the Hamiltonian of the electrons in the QW has the form:

$$H = \sum_{\sigma\sigma'} \int dx \psi_{\sigma}^{\dagger}(x) \left\{ -\frac{\nabla^2}{2m^*} \delta_{\sigma\sigma'} + [g\mu_B \mathbf{B} + \mathbf{h}(-i\nabla)] \cdot \frac{\vec{\sigma}_{\sigma\sigma'}}{2} + \Psi(\mathbf{r}) \right\} \psi_{\sigma'}(x) + \frac{1}{2} \sum_{\sigma\sigma'} \int dx_1 dx_2 \psi_{\sigma}^{\dagger}(x_1) \psi_{\sigma'}^{\dagger}(x_2) V(\mathbf{r}_1 - \mathbf{r}_2) \psi_{\sigma'}(x_2) \psi_{\sigma}(x_1) + H_I , \quad (1)$$

where  $\psi_{\sigma}(x)$  is an electron field operator with spin  $z$ -component  $\sigma$ .  $x = (\mathbf{r}, t)$ .  $\vec{\sigma}$  are the Pauli matrices.

In QW system, the DP term is composed of the Dresselhaus term<sup>23</sup> and the Rashba term<sup>24,25</sup>. The Dresselhaus term is due to the lack of inversion symmetry in the zinc-blend crystal Brillouin zone and is sometimes referred to as bulk inversion asymmetry (BIA) term. For the (100) GaAs QW system, it can be written as<sup>26,27</sup>

$$\begin{aligned} h_x^{\text{BIA}}(\mathbf{k}) &= \gamma k_x (k_y^2 - \langle k_z^2 \rangle), \\ h_y^{\text{BIA}}(\mathbf{k}) &= \gamma k_y (\langle k_z^2 \rangle - k_x^2), \\ h_z^{\text{BIA}}(\mathbf{k}) &= 0 . \end{aligned} \quad (2)$$

Here  $\langle k_z^2 \rangle$  represents the average of the operator  $-(\frac{\partial}{\partial z})^2$  over the electronic state of the lowest subband and is therefore  $(\pi/a)^2$ .  $\gamma = (4/3)(m^*/m_{cv})(1/\sqrt{2m^*E_g})(\eta/\sqrt{1-\eta/3})$  and  $\eta = \Delta/(E_g + \Delta)$ , in which  $E_g$  denotes the band gap;  $\Delta$  represents the spin-orbit splitting of the valence band;  $m^*$  stands for the electron mass in GaAs; and  $m_{cv}$  is a constant close in magnitude to free electron mass  $m_0$ <sup>28</sup>. The Rashba term appears if the self-consistent potential within a QW is asymmetric along the growth direction and is therefore referred to as structure inversion asymmetry (SIA) contribution. It can be written as

$$h_x^{\text{SIA}}(\mathbf{k}) = \alpha k_y, \quad h_y^{\text{SIA}}(\mathbf{k}) = -\alpha k_x, \quad h_z^{\text{SIA}}(\mathbf{k}) = 0. \quad (3)$$

In these equations,  $\alpha$  is proportional to the interface electric field  $E_z$  along the growth direction:

$$\alpha = \alpha_0 e E_z, \quad (4)$$

with the coefficient  $\alpha_0$  being inversely proportional to the energy gap and the effective mass<sup>29</sup>. For QW's composed of narrow band-gap semiconductors such as InAs, the Rashba term is the main spin-dephasing mechanism; whereas for QW's of wide band-gap semiconductors such as GaAs, the Dresselhaus term is dominant.

$\Psi(\mathbf{r})$  in Eq. (1) is the electric potential. It satisfies the Poisson equation

$$\nabla_{\mathbf{r}}^2 \Psi(\mathbf{r}, t) = -e[n(\mathbf{r}, t) - n_0(\mathbf{r})]/\varepsilon_0, \quad (5)$$

where  $\varepsilon_0$  is the static dielectric constant.  $n(\mathbf{r}, t) = \sum_{\sigma} \langle \psi_{\sigma}^{\dagger}(x) \psi_{\sigma}(x) \rangle$  is the electron density at position  $\mathbf{r}$  and time  $t$ .  $n_0(\mathbf{r})$  denotes the background positive charge density.

The second term in Eq. (1) is the electron-electron Coulomb interaction  $H_{ee}$ , with  $V(\mathbf{r})$  standing for the Coulomb potential. The interaction Hamiltonian  $H_I$  is composed of electron-longitudinal optical (LO) phonon interaction  $H_{LO}$ , electron-acoustic (AC) phonon interaction  $H_{AC}$ , as well as electron-impurity scattering  $H_i$ . Their expressions can be found in Refs. 30 and 31.

By using the nonequilibrium Green function method with gradient expression as well as the generalized Kadanoff-Baym Ansatz, we construct the kinetic Bloch equations as follows:

$$\frac{\partial \rho(\mathbf{R}, \mathbf{k}, t)}{\partial t} - \frac{1}{2} \{ \nabla_{\mathbf{R}} \bar{\varepsilon}(\mathbf{R}, \mathbf{k}, t), \nabla_{\mathbf{k}} \rho(\mathbf{R}, \mathbf{k}, t) \} + \frac{1}{2} \{ \nabla_{\mathbf{k}} \bar{\varepsilon}(\mathbf{R}, \mathbf{k}, t), \nabla_{\mathbf{R}} \rho(\mathbf{R}, \mathbf{k}, t) \} - \frac{\partial \rho(\mathbf{R}, \mathbf{k}, t)}{\partial t} \Big|_c = \frac{\partial \rho(\mathbf{R}, \mathbf{k}, t)}{\partial t} \Big|_s. \quad (6)$$

Here  $\rho(\mathbf{R}, \mathbf{k}, t)$  represents the single particle density matrix. The diagonal elements describe the electron distribution functions  $\rho_{\sigma\sigma}(\mathbf{R}, \mathbf{k}, t) = f_{\sigma}(\mathbf{R}, \mathbf{k}, t)$  of wave vector  $\mathbf{k}$  and spin  $\sigma (\sigma = \pm \frac{1}{2})$  at position  $\mathbf{R}$  and time  $t$ . The off-diagonal elements  $\rho_{\sigma-\sigma}(\mathbf{R}, \mathbf{k}, t)$  are the inter-spin-band polarization components (we refer it as spin coherences in our paper) for the spin coherence. The quasi-particle energy  $\bar{\varepsilon}(\mathbf{R}, \mathbf{k}, t)$  take the following forms:

$$\bar{\varepsilon}_{\sigma\sigma'}(\mathbf{R}, \mathbf{k}, t) = \varepsilon_{\mathbf{k}} \delta_{\sigma\sigma'} + [g\mu_B \mathbf{B} + \mathbf{h}(\mathbf{k})] \cdot \frac{\vec{\sigma}_{\sigma\sigma'}}{2} - e\Psi(\mathbf{R}, t) + \Sigma_{\sigma\sigma'}(\mathbf{R}, \mathbf{k}, t). \quad (7)$$

Here  $\varepsilon_{\mathbf{k}} = \mathbf{k}^2/2m^*$  is the energy spectrum of the electron.  $\Sigma_{\sigma\sigma'}(\mathbf{R}, \mathbf{k}, t) = -\sum_{\mathbf{q}} V_{\mathbf{q}}(\mathbf{R}, t) \rho_{\sigma\sigma'}(\mathbf{R}, \mathbf{k} - \mathbf{q}, t)$  is the Hartree-Fock energy, with  $V_{\mathbf{q}}(\mathbf{R}, t)$  denoting the Coulomb matrix element. In 2D case,  $V_{\mathbf{q}}(\mathbf{R}, t)$  is given by

$$V_{\mathbf{q}}(\mathbf{R}, t) = \sum_{q_z} \frac{4\pi e^2}{\epsilon_0 [\mathbf{q}^2 + q_z^2 + \kappa^2(\mathbf{R}, t)]} |I(iq_z)|^2, \quad (8)$$

$$\frac{\partial \rho_{\sigma-\sigma}(\mathbf{R}, \mathbf{k}, t)}{\partial t} \Big|_c = i[\bar{\varepsilon}_{\sigma\sigma}(\mathbf{R}, \mathbf{k}, t) - \bar{\varepsilon}_{-\sigma-\sigma}(\mathbf{R}, \mathbf{k}, t)] \rho_{\sigma-\sigma}(\mathbf{R}, \mathbf{k}, t) + i\bar{\varepsilon}_{\sigma-\sigma}(\mathbf{R}, \mathbf{k}, t) [f_{-\sigma}(\mathbf{R}, \mathbf{k}, t) - f_{\sigma}(\mathbf{R}, \mathbf{k}, t)] \quad (10)$$

for the spin coherences respectively. The scattering terms in the Markovian limit read

$$\begin{aligned} \frac{\partial f_{\sigma}(\mathbf{R}, \mathbf{k}, t)}{\partial t} \Big|_s &= \left\{ -2\pi \sum_{\mathbf{q}q_z\lambda} |g_{\mathbf{q}q_z\lambda}|^2 \delta(\varepsilon_{\mathbf{k}} - \varepsilon_{\mathbf{k}-\mathbf{q}} - \Omega_{\mathbf{q}q_z\lambda}) \left[ N_{\mathbf{q}q_z\lambda} (f_{\sigma}(\mathbf{R}, \mathbf{k}, t) - f_{\sigma}(\mathbf{R}, \mathbf{k} - \mathbf{q}, t)) \right. \right. \\ &\quad + f_{\sigma}(\mathbf{R}, \mathbf{k}, t) (1 - f_{\sigma}(\mathbf{R}, \mathbf{k} - \mathbf{q}, t)) - \text{Re}(\rho_{\sigma-\sigma}(\mathbf{R}, \mathbf{k}, t) \rho_{\sigma-\sigma}^*(\mathbf{R}, \mathbf{k} - \mathbf{q}, t)) \Big] \\ &\quad - 2\pi N_i \sum_{\mathbf{q}} U_{\mathbf{q}}^2 \delta(\varepsilon_{\mathbf{k}} - \varepsilon_{\mathbf{k}-\mathbf{q}}) \left[ f_{\sigma}(\mathbf{R}, \mathbf{k}, t) (f_{\sigma}(\mathbf{R}, \mathbf{k} - \mathbf{q}, t)) - \text{Re}(\rho_{\sigma-\sigma}(\mathbf{R}, \mathbf{k}, t) \right. \\ &\quad \times \rho_{\sigma-\sigma}^*(\mathbf{R}, \mathbf{k} - \mathbf{q}, t)) \Big] - 2\pi \sum_{\mathbf{k}'\mathbf{q}\sigma'} V_{\mathbf{q}}^2 \delta(\varepsilon_{\mathbf{k}-\mathbf{q}} - \varepsilon_{\mathbf{k}} + \varepsilon_{\mathbf{k}'} - \varepsilon_{\mathbf{k}'-\mathbf{q}}) \\ &\quad \times \left[ (1 - f_{\sigma}(\mathbf{R}, \mathbf{k} - \mathbf{q}, t)) f_{\sigma}(\mathbf{R}, \mathbf{k}, t) (1 - f_{\sigma'}(\mathbf{R}, \mathbf{k}', t)) f_{\sigma'}(\mathbf{R}, \mathbf{k}' - \mathbf{q}, t) \right. \\ &\quad - f_{\sigma}(\mathbf{R}, \mathbf{k} - \mathbf{q}, t) (1 - f_{\sigma}(\mathbf{R}, \mathbf{k}, t)) f_{\sigma'}(\mathbf{R}, \mathbf{k}', t) (1 - f_{\sigma'}(\mathbf{R}, \mathbf{k}' - \mathbf{q}, t)) \\ &\quad + \text{Re}(\rho_{\sigma-\sigma}(\mathbf{R}, \mathbf{k} - \mathbf{q}, t) \rho_{-\sigma\sigma}(\mathbf{R}, \mathbf{k}, t)) (f_{\sigma'}(\mathbf{R}, \mathbf{k}', t) - f_{\sigma'}(\mathbf{R}, \mathbf{k}' - \mathbf{q}, t)) \\ &\quad + \text{Re}(\rho_{\sigma'-\sigma'}(\mathbf{R}, \mathbf{k}', t) \rho_{-\sigma'\sigma'}(\mathbf{R}, \mathbf{k}' - \mathbf{q}, t)) (f_{\sigma}(\mathbf{R}, \mathbf{k}, t) - f_{\sigma}(\mathbf{R}, \mathbf{k} - \mathbf{q}, t)) \Big] \Big\} \\ &\quad - \left\{ \mathbf{k} \leftrightarrow \mathbf{k} - \mathbf{q}, \mathbf{k}' \leftrightarrow \mathbf{k}' - \mathbf{q} \right\} \end{aligned} \quad (11)$$

and

$$\begin{aligned} \frac{\partial \rho_{\sigma-\sigma}(\mathbf{R}, \mathbf{k}, t)}{\partial t} \Big|_s &= \left\{ -\pi \sum_{\mathbf{q}q_z\lambda} g_{\mathbf{q}q_z\lambda}^2 \delta(\varepsilon_{\mathbf{k}} - \varepsilon_{\mathbf{k}-\mathbf{q}} - \Omega_{\mathbf{q}q_z\lambda}) \left[ (f_{\sigma}(\mathbf{R}, \mathbf{k}, t) + f_{-\sigma}(\mathbf{R}, \mathbf{k}, t)) \rho_{\sigma-\sigma}(\mathbf{R}, \mathbf{k} - \mathbf{q}, t) \right. \right. \\ &\quad \left. \left. - f_{-\sigma}(\mathbf{R}, \mathbf{k} - \mathbf{q}, t) (f_{\sigma}(\mathbf{R}, \mathbf{k}, t) + f_{-\sigma}(\mathbf{R}, \mathbf{k}, t)) \rho_{\sigma-\sigma}^*(\mathbf{R}, \mathbf{k} - \mathbf{q}, t) \right] \right\} \end{aligned}$$

$$\begin{aligned}
& + (f_\sigma(\mathbf{R}, \mathbf{k} - \mathbf{q}, t) + f_{-\sigma}(\mathbf{R}, \mathbf{k} - \mathbf{q}, t) - 2) \rho_{\sigma-\sigma}(\mathbf{R}, \mathbf{k}, t) - 2N_{\mathbf{q}q_z\lambda} (\rho_{\sigma-\sigma}(\mathbf{R}, \mathbf{k}, t) - \rho_{\sigma-\sigma}(\mathbf{R}, \mathbf{k} - \mathbf{q}, t)) \\
& - \pi N_i \sum_{\mathbf{q}\lambda} U_{\mathbf{q}}^2 \delta(\varepsilon_{\mathbf{k}} - \varepsilon_{\mathbf{k}-\mathbf{q}}) \left[ (f_\sigma(\mathbf{R}, \mathbf{k}, t) + f_{-\sigma}(\mathbf{R}, \mathbf{k}, t)) \rho_{\sigma-\sigma}(\mathbf{R}, \mathbf{k} - \mathbf{q}, t) \right. \\
& - (2 - f_\sigma(\mathbf{R}, \mathbf{k} - \mathbf{q}, t) f_{-\sigma}(\mathbf{R}, \mathbf{k} - \mathbf{q}, t)) \rho_{\sigma-\sigma}(\mathbf{R}, \mathbf{k}, t) \\
& - \pi \sum_{\mathbf{k}'\mathbf{q}\sigma'} V_{\mathbf{q}}^2 \pi \delta(\varepsilon_{\mathbf{k}-\mathbf{q}} - \varepsilon_{\mathbf{k}} + \varepsilon_{\mathbf{k}'} - \varepsilon_{\mathbf{k}'-\mathbf{q}}) \left\{ (f_\sigma(\mathbf{R}, \mathbf{k} - \mathbf{q}, t) \rho_{\sigma-\sigma}(\mathbf{R}, \mathbf{k}, t) + \rho_{\sigma-\sigma}(\mathbf{R}, \mathbf{k} - \mathbf{q}, t) f_{-\sigma}(\mathbf{R}, \mathbf{k}, t)) \right. \\
& \times (f_{\sigma'}(\mathbf{R}, \mathbf{k}', t) - f_{\sigma'}(\mathbf{R}, \mathbf{k}' - \mathbf{q}, t)) \\
& + \rho_{\sigma-\sigma}(\mathbf{R}, \mathbf{k}, t) \left[ (1 - f_\sigma(\mathbf{R}, \mathbf{k}', \sigma', t)) f_{\sigma'}(\mathbf{R}, \mathbf{k}' - \mathbf{q}, t) - \rho_{\sigma'-\sigma'}(\mathbf{R}, \mathbf{k}', t) \rho_{-\sigma'\sigma'}(\mathbf{R}, \mathbf{k}' - \mathbf{q}, t) \right] \\
& \left. - \rho_{\sigma-\sigma}(\mathbf{R}, \mathbf{k} - \mathbf{q}, t) \left[ f_{\sigma'}(\mathbf{R}, \mathbf{k}' - \mathbf{q}, t) (1 - f_{\sigma'}(\mathbf{R}, \mathbf{k} - \mathbf{q}, t)) - \rho_{\sigma'-\sigma'}(\mathbf{R}, \mathbf{k}', t) \rho_{-\sigma'\sigma'}(\mathbf{R}, \mathbf{k}' - \mathbf{q}, t) \right] \right\} \\
& - \left\{ \mathbf{k} \leftrightarrow \mathbf{k} - \mathbf{q}, \mathbf{k}' \leftrightarrow \mathbf{k}' - \mathbf{q} \right\}. \tag{12}
\end{aligned}$$

In these equations,  $g_{\mathbf{q}q_z\lambda}$  and  $N_{\mathbf{q}q_z\lambda}$  are the electron-phonon matrix element and the phonon distribution function with branch  $\lambda$  and wavevector  $\mathbf{Q} = (\mathbf{q}, q_z)$ , respectively.  $N_i$  is the concentration of impurities in the QW and  $U_{\mathbf{q}}$  is the matrix element of electron-impurity interaction.

Equations (6)–(12) combined with certain boundary and initial conditions comprise the complete set of kinetic equations of our investigation.

### III. SIMPLIFIED KINETIC EQUATIONS

The general kinetics equations are too complicated to solve analytically. Here we first consider two simplified cases where one can get the exact solutions.

We first reduce the kinetic Bloch equations (6) to those in the independent electron approach. This can be done as follows: The DP mechanism forms an effective magnetic field. It can flip the spin up electrons to spin down ones, and vice versa. The DP term combines with the scattering will result in a longitudinal spin dephasing. By applying the relaxation time approximation to describe this dephasing and discarding the spin coherences  $\rho_{\sigma-\sigma}(\mathbf{R}, \mathbf{k}, t)$  as well as the DP term (to avoid double counting of the DP mechanism), one obtains the simplified Bloch equations

$$\begin{aligned}
\frac{\partial f_\sigma(\mathbf{R}, \mathbf{k}, t)}{\partial t} & - \nabla_{\mathbf{R}} \bar{\varepsilon}_{\sigma\sigma}(\mathbf{R}, \mathbf{k}, t) \cdot \nabla_{\mathbf{k}} f_\sigma(\mathbf{R}, \mathbf{k}, t) \\
& - \nabla_{\mathbf{k}} \bar{\varepsilon}_{\sigma\sigma}(\mathbf{R}, \mathbf{k}, t) \cdot \nabla_{\mathbf{R}} f_\sigma(\mathbf{R}, \mathbf{k}, t) \\
& = - \frac{f_\sigma(\mathbf{R}, \mathbf{k}, t) - f_0(\mathbf{R}, \mathbf{k})}{\tau_s}, \tag{13}
\end{aligned}$$

with  $f_0(\mathbf{R}, \mathbf{k})$  representing the distribution function of electrons in equilibrium state. After carrying out the summation over  $\mathbf{k}$ , one gets the equation of continuity for electrons of spin  $\sigma$ ,

$$\frac{\partial n_\sigma(\mathbf{R}, t)}{\partial t} - \frac{1}{e} \nabla_{\mathbf{R}} \cdot \mathbf{J}_\sigma(\mathbf{R}, t) = - \frac{n_\sigma(\mathbf{R}, t) - n_0(\mathbf{R})}{\tau_s}, \tag{14}$$

in which  $n_\sigma(\mathbf{R}, t) = \sum_{\mathbf{k}} f_\sigma(\mathbf{R}, \mathbf{k}, t)$  is the density of electrons with spin  $\sigma$  at position  $\mathbf{R}$  and time  $t$  and  $n_0(\mathbf{R}) = \sum_{\mathbf{k}} f_0(\mathbf{R}, \mathbf{k})$  is the corresponding electron density at equilibrium state.  $\mathbf{J}_\sigma(\mathbf{R}, t) = \sum_{\mathbf{k}} (-e) \mathbf{v}_{\sigma\mathbf{k}} f_\sigma(\mathbf{R}, \mathbf{k}, t)$  is the electric current of spin  $\sigma$ . The spin dependent velocity is  $\mathbf{v}_{\sigma\mathbf{k}} = \nabla_{\mathbf{k}} \bar{\varepsilon}_{\sigma\sigma}(\mathbf{R}, \mathbf{k}, t)$ .  $\mathbf{J}_\sigma(\mathbf{R}, t)$  can be obtained by multiplying  $\mathbf{v}_{\sigma\mathbf{k}}$  to the Bloch equations and then carrying out the summation over  $\mathbf{k}$  from both sides of the equations. By applying the relaxation time approximation to describe the momentum scattering and keeping terms of the lowest order (*i.e.*, neglecting terms containing  $\rho_{\sigma-\sigma}$ ), one obtains the expression for the current in the steady state:

$$\mathbf{J}_\sigma(\mathbf{R}, t) = n_\sigma(\mathbf{R}, t) e \mu \mathbf{E}(\mathbf{R}, t) + e D \nabla_{\mathbf{R}} n_\sigma(\mathbf{R}, t), \tag{15}$$

where  $\mu$  and  $D$  represent the electron mobility and diffusion constant separately. Equations (14) and (15) are the diffusion equations in the independent electron approach<sup>10,11,13,16</sup>. The solution for the diffusion equations shows that the spin signal decays exponentially along the diffusion direction as  $e^{-x/\sqrt{D\tau_s}}$ . This decay is due to the dephasing caused by the DP term together with the scattering.

One can see from the derivation of above diffusion equations that, by summing over  $\mathbf{k}$ , the  $\mathbf{k}$  dependence of the coefficients of  $\nabla_{\mathbf{R}} \rho(\mathbf{R}, \mathbf{k}, t)$  in the Bloch equations (6) is removed. This will not cause any problem when there is no spin precession in the diffusion. However, when the electron spin precesses along the diffusion in the presence of a magnetic field or an effective one (*i.e.*, the DP term), this kind of  $\mathbf{k}$  dependence may cause additional spin decoherence.

To reveal this effect, we now study a much simplified case for the Bloch equations by neglecting the DP terms

$\mathbf{h}(\mathbf{k})$ , the self energies as well as the scattering in Eq. (6). We assume the spin diffusion is along the  $x$ -axis. When the applied electric field is zero, in the steady state the simplified equations are therefore given by

$$\frac{k_x}{m^*} \partial_x f_\sigma(x, \mathbf{k}) + g\mu_B B \text{Im}[\rho_{\sigma, -\sigma}(x, \mathbf{k})] = 0, \quad (16)$$

$$\frac{k_x}{m^*} \partial_x \rho_{\sigma-\sigma}(x, \mathbf{k}) - i \frac{g\mu_B B}{2} \Delta f_\sigma(x, \mathbf{k}) = 0. \quad (17)$$

Here we take the magnetic field  $\mathbf{B}$  along the  $x$ -axis.  $\Delta f_\sigma(x, \mathbf{k}) = f_\sigma(x, \mathbf{k}) - f_{-\sigma}(x, \mathbf{k})$ . For the boundary condition, we assume that the electron distribution functions at  $x = 0$  are the Fermi distributions

$$f_\sigma(0, \mathbf{k}) = f_\sigma^0(\mathbf{k}) = \{\exp[(\varepsilon_{\mathbf{k}} - \mu_\sigma)/T] + 1\}^{-1}, \quad (18)$$

with  $T$ , the temperature and  $\mu_\sigma$ , the electron chemical potential of spin  $\sigma$ . The spin coherence is assumed to be zero at  $x = 0$ :

$$\rho_{\sigma-\sigma}(0, \mathbf{k}) \equiv 0. \quad (19)$$

The solution of this simplified equations with the boundary conditions (18) and (19) can be written out directly as follows:

$$\Delta f_\sigma(x, \mathbf{k}) = \Delta f^0(\mathbf{k}) \cos \frac{g\mu_B B m^* x}{k_x}, \quad (20)$$

$$\rho_{\sigma-\sigma}(x, \mathbf{k}) = \frac{i}{2} \Delta f^0(\mathbf{k}) \sin \frac{g\mu_B B m^* x}{k_x}. \quad (21)$$

Equations (20) and (21) clearly show the effect of the  $k$ -dependence to the spin precession along the diffusion direction. For each fixed  $k_x$ , the spin precesses along the diffusion direction with fixed period without any decay. Nevertheless, for different  $k_x$  the period is different. The total difference of the electron densities with different spin is the summation over all wavenumbers  $\Delta N = \sum_{\mathbf{k}} \Delta f_\sigma(x, \mathbf{k})$ . It is noted that the phase at the contact  $x = 0$  for different  $k_x$  is all the same. However, the speed of the phase of spin precession is different for different  $k_x$ . Consequently, when  $x$  is large enough, spins with different phases may cancel each other.

This can further be seen from Fig. 1 where the electron densities  $N_\sigma = \sum_{\mathbf{k}} f_\sigma(x, \mathbf{k})$  for up and down spin are plotted as functions of position  $x$ . The boundary electron densities at  $x = 0$  are  $N_{1/2}(0) = 2.05 \times 10^{11} \text{ cm}^{-2}$  and  $N_{-1/2}(0) = 1.95 \times 10^{11} \text{ cm}^{-2}$ . We take  $B = 1 \text{ T}$  and  $T = 200 \text{ K}$ . In order to show the transverse spin dephasing, we plot in the same figure the incoherently summed spin coherence  $\rho(t) = \sum_{\mathbf{k}} |\rho_{\frac{1}{2}-\frac{1}{2}}(x, \mathbf{k})|$ . It is understood that both the true dissipation and the interference among the  $\mathbf{k}$  states may contribute to the decay. We refer this decay as decoherence. The decay due to interference is caused by the different precession speed between electrons with different wavevector. For finite system, this leads to reversible loss of coherence among electrons. Whereas for the true dissipation, the coherence

is lost permanently<sup>32,33</sup>. Dephasing is used to describe this irreversible decoherence. The incoherent summation is therefore used to isolate the irreversible decay from the decay caused by interference<sup>20,32</sup>. From the figure, one can see clearly the longitudinal decoherence caused by the interference effect. It is also noted from the figure that  $\rho$  does not decay with the distance. This is consistent with the fact that there is no scattering in Eqs. (20) and (21) and the decay comes from the interference effect. From this simplified model, one can conclude that although the QIEM is very successful in describing the spin-degenerate electron transport/diffusion for decays, it is inadequate to study the spin transport problem. Therefore, it is important to use the full many-body theory to study the spin transport.

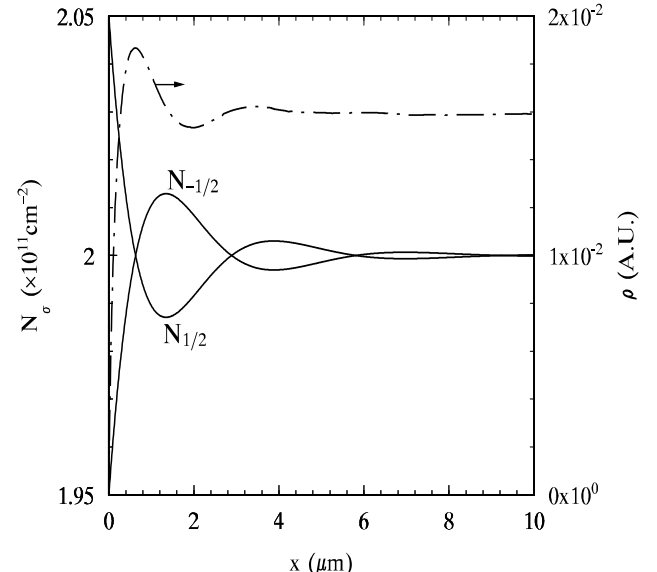


FIG. 1. Electron densities of up spin and down spin (solid curves) and the incoherently summed spin coherence  $\rho$  (dashed curve) versus the diffusion length  $x$ .  $B = 1 \text{ T}$ . Note the scale of the spin coherence is on the right side of the figure.

#### IV. SPIN DIFFUSION IN THE STEADY STATE

We now turn to the spin diffusion problem of a GaAs QW with the DP term, selfenergy and scattering included. The direction of the diffusion is perpendicular to the QW growth direction ( $z$ -axis). The kinetic Bloch equations (6)–(12) together with the Poisson equation (5) are numerically solved iteratively<sup>34,35</sup> to achieve the self-consistent solution. In the present study, we only include electron-phonon and electron-impurity scatterings in Eqs. (11) and (12). Electron-electron scattering is not included in this first stage of computation. It is understood that this approximation will only bring marginal effect to the spin dephasing when the spin polarization is

small. Also the spin Coulomb drag effect is small if the temperature is away from Fermi temperature<sup>36</sup>. Therefore, the investigation here will be limited to the small spin polarization and the temperature away from the Fermi temperature. As we concentrate on relatively high temperature regime in the present study, for electron-phonon scattering one only needs to include electron-LO phonon scattering.

The matrix element of electron-LO phonon scattering is given by  $g_{qqz}^2 = 4\pi\beta\omega_0^{3/2}|I(iq_z)|^2/[\sqrt{2\mu}(q^2 + q_z^2)]$  with  $\beta = e^2\sqrt{\mu/(2\omega_0)}(\epsilon_\infty^{-1} - \epsilon_0^{-1})$ .  $\epsilon_\infty$  is the optical dielectric constant, and  $\omega_0$  is the optical phonon frequency. The matrix element of electron-impurity interaction reads  $U_q^2 = \sum_{q_z} \{4\pi Z_i e^2/[\epsilon_0(q^2 + q_z^2)]\}^2 |I(iq_z)|^2$ , with  $Z_i$  standing for the electric charge of impurity.

The QW width is chosen typically to be 7.5 nm. The material parameters of GaAs in our calculation are tabulated in Table I<sup>37</sup>. As GaAs is a wide bandgap semiconductor, the dominant spin dephasing comes from the Dresselhaus term. Therefore, the Rashba term is omitted in the calculation unless specified.

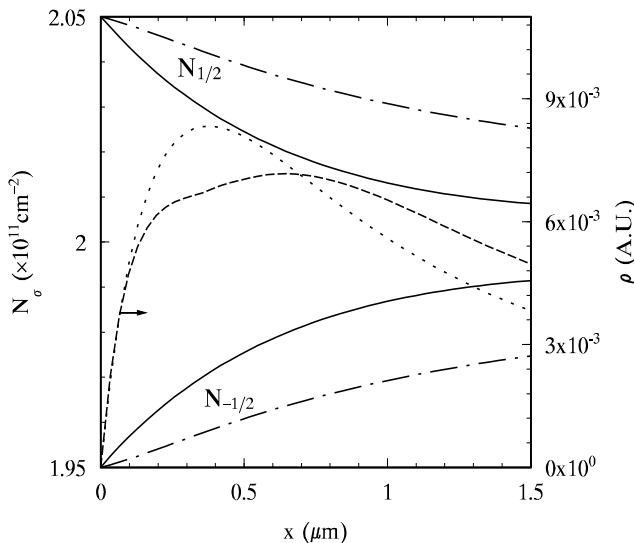


FIG. 2. Electron densities of up spin and down spin and the incoherently summed spin coherence versus the diffusion length  $x$ . Solid curves and dashed curve:  $N_\sigma$  and  $\rho$  from the full Bloch equations; Dash-dotted curves and dotted curve:  $N_\sigma$  and  $\rho$  from the equations without the interference effect. Note the scale of the spin coherence is on the right side of the figure.

We first study the spin diffusion along the  $x$ -axis in the steady state under a constant injection of spin polarized current at  $x = 0$ . The boundary is assumed to be Ohmic contact. We further restrict ourselves to the linear transport region, *i.e.* the applied electric field is small that the hot electron effect is not important. For this system, the electron distribution function at the boundary

is assumed to be drifted Fermi distribution,

$$f_\sigma(0, \mathbf{k}, t) \equiv f_\sigma^0(\mathbf{k}) = \frac{1}{\exp[(\epsilon_{\mathbf{k}-m^*\mathbf{v}_d} - \mu_\sigma)/T] + 1}, \quad (22)$$

in which  $\mathbf{v}_d = \mu\mathbf{E}$  is the drift velocity.  $\mu$  is the linear electron mobility, whose expression is given by various authors<sup>38,39</sup>. The spin coherences at boundary are assumed to be zero

$$\rho_{\sigma-\sigma}(0, \mathbf{k}, t) \equiv 0. \quad (23)$$

It is understood that the boundary condition here is an approximation to describe the distributions just after the injection of the *spin polarization* from the Ohmic contact. There is no net charge injection into the QW and the well is kept charge natural everywhere. Actually, this boundary condition does not necessarily come from the injection at the interface. It can also be produced in the center of semiconductors by a circularly polarized cw laser.

The main results are plotted in Figs. 2 to 8. In these figures, the total electron density in the two spin bands is  $N_e = 4 \times 10^{11} \text{ cm}^{-2}$ , whereas the density in the spin-up band is  $0.1 \times 10^{11} \text{ cm}^{-2}$  higher than the spin down band at  $x = 0$ . This polarization is in the same order of the spin injection rate from ferromagnet achieved to-date<sup>40</sup>. The computation is carried out in a parallel manner in the “Beowulf” cluster. For a typical calculation, it takes about 60 hours to get a curve with 16-node AMD Athlon XP1800+ CPU’s.

#### A. $\mathbf{E}=\mathbf{0}$ case

In Fig. 2 we plot the electron densities in the spin-up and -down bands as a function of the position for  $N_i = 0$  and the applied electric field  $E = 0$ . It is seen from the figure that the surplus of the spin up electrons decreases rapidly along the direction of the diffusion, similar to the simplified model shown above. The fast decay is understood mainly from the decoherence originated from the interference effect due to the inhomogeneous broadening as in the evolution equation of  $\rho_{\sigma\sigma'}(\mathbf{R}, \mathbf{k}, t)$  [Eq. (6)], the coefficients of  $\partial_x \rho_{\sigma\sigma'}$ ,  $\partial_x \rho_{\sigma-\sigma'}$  and  $\partial_x \rho_{-\sigma\sigma'}$ :

$$\frac{k_x}{m^*} + \frac{1}{2} \partial_{k_x} [\Sigma_{\sigma\sigma}(\mathbf{R}, \mathbf{k}, t) + \Sigma_{\sigma'\sigma'}(\mathbf{R}, \mathbf{k}, t)], \quad (24)$$

$$\frac{1}{2} \partial_{k_x} [h_x(\mathbf{k}) + i\sigma h_y(\mathbf{k}) + \Sigma_{\sigma-\sigma}(\mathbf{R}, \mathbf{k}, t)], \quad (25)$$

$$\frac{1}{2} \partial_{k_x} [h_x(\mathbf{k}) - i\sigma' h_y(\mathbf{k}) + \Sigma_{-\sigma'\sigma'}(\mathbf{R}, \mathbf{k}, t)], \quad (26)$$

are all  $k$ -dependent. Other dephasing effects such as those caused by the DP terms in Eqs. (9) and (10) together with the spin conserving LO phonon scattering also contribute to the decay. Besides, we pointed out that the inhomogeneous broadening effect combined with spin-conserving scattering can also cause spin

dephasing<sup>20</sup>. Therefore, above mentioned inhomogeneous broadening may also cause spin dephasing in the presence of LO phonon scattering. To compare the decoherence due to interference and the dephasing due to the DP term together with the scattering, we remove the interference effect in the transport equations by replacing  $k$  in the coefficients [Eqs. (24)-(26)] with  $k = k_F$ . Here  $k_F$  represents the Fermi wavevector. Therefore, if there is any decay of spin polarization along the diffusion direction, it comes from the spin dephasing. The numerical result is plotted in Fig. 2. It is shown clearly that the decay of spin polarization due to the dephasing effect alone (dash-dotted curves) is much slower than that due to the interference-induced decoherence. In the figure we also plot the corresponding incoherently summed spin coherences  $\rho$ . One can see from the figure that both coherences  $\rho$  decay slowly and their decay rates are comparable when  $x > 1 \mu\text{m}$ . This further justifies what mentioned above that the fast decay of the spin polarization is mainly due to the interference effect.

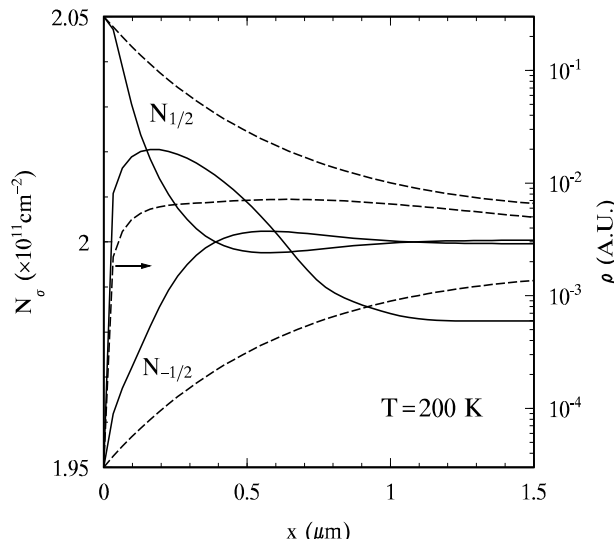


FIG. 3. Electron densities of up spin and down spin and the incoherently summed spin coherence versus the diffusion length  $x$  for different applied magnetic field with  $N_i = 0$ . Solid curves:  $N_\sigma$  and  $\rho$  for  $B = 2 \text{ T}$ ; Dashed curves:  $N_\sigma$  and  $\rho$  for  $B = 0$ . Note the scale of the spin coherence is on the right side of the figure.

We next investigate the spin diffusion with a magnetic field applied in the Voigt configuration (along the  $x$ -axis). The result for  $B = 2 \text{ T}$  at  $T = 200 \text{ K}$  is plotted in Fig. 3 as solid curves. It is seen from the figure that, the spin-up electrons flip to the spin-down ones along the direction of diffusion due to the presence of the magnetic field. The density of spin-up electron decreases first along the diffusion direction. At the distant of about  $0.6 \mu\text{m}$  away from the interface, the density of spin-up electrons arrives its minimum; and then increases to reach the equilibrium.

The electron densities of the two spin bands have a crossing at the distant of  $0.4 \mu\text{m}$  away from the interface. By comparing the results with (solid curves) and without (dashed curves) the applied magnetic field, one can see that the decay rate of the exceeded electron density in the presence of the magnetic field is much faster than that without the field. In the presence of the magnetic field the difference between the densities of two spin band almost vanishes after the first oscillation ( $1 \mu\text{m}$ ). This effect is also mainly due to the interference effect. One can see from our simplified model that the oscillation along  $x$ -axis of the electron with wave vector  $\mathbf{k}$  is characterized by the “frequency”  $g\mu_B B m^*/k_x$  which is proportional to the magnetic field. The larger the magnetic field is, the stronger the interference effect gets. With the applied magnetic field as large as  $2 \text{ T}$ , the “frequency” is dominated by the magnetic field. Whereas when the applied magnetic field is very small or absent, the “frequency” is controlled by the effective magnetic field  $B_{\text{eff}} = |h(\mathbf{k})|/g$  resulting from the DP term. This effective magnetic field is much smaller than  $1 \text{ T}$  especially at the small wavevectors. Therefore the decay of spin signal in the presence of magnetic field is much faster than that without the magnetic field. One further notices that the magnetic field does not affect the decay which is originated from the dephasing effect. This can be seen from the incoherently summed spin coherences, which are also plotted in Fig. 3, that the decay rates after  $x > 1 \mu\text{m}$  are almost the same for both cases of  $B = 0$  and  $B = 2 \text{ T}$ .

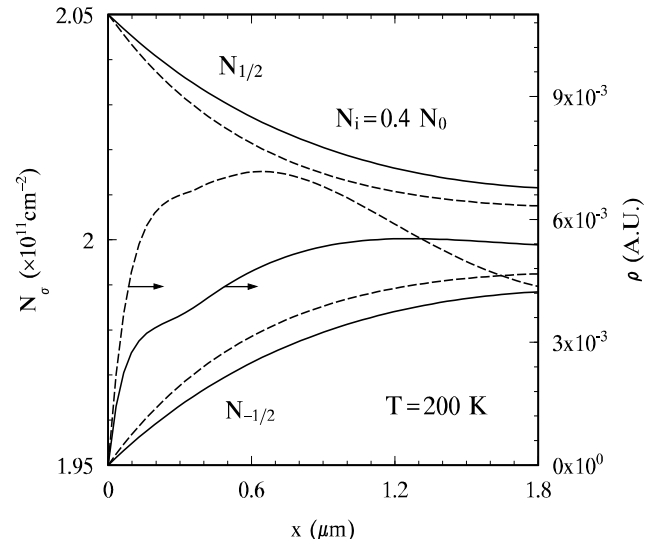


FIG. 4. Electron densities of up spin and down spin and the incoherently summed spin coherence versus the diffusion length  $x$  for different impurities levels. Solid curves:  $N_\sigma$  and  $\rho$  for  $N_i = 0.4N_0$ . Dashed curves:  $N_\sigma$  and  $\rho$  for  $N_i = 0$ . Note the scale of the spin coherence is on the right side of the figure.

In Fig. 4, the densities of two spin bands as well as

the incoherently summed spin coherence  $\rho$  are plotted as solid curves against the position  $x$  for a QW with  $N_i = 0.4N_e$ . For comparison, the corresponding results for pure sample, which have been plotted in Fig. 2, are also given as dashed curves. It has been argued in the current simplified models<sup>11,41</sup> that the inclusion of impurities would reduce the injection length, as the impurities will shorten the electron mean free path and therefore decrease the diffusion constant and the spin diffusion length. One can clearly see from Fig. 4 that contrary to what predicted before, *the injection length is enlarged by the impurity*. This is because that the simplified treatment only takes into account of one aspect of the role of impurities, *i.e.*, the mean free path of electrons, but totally ignores the fact that impurities also affect spin dephasing time. Studies of the spin dephasing in  $n$ -doped GaAs have show that the spin dephasing time is increased by the impurities<sup>21,42</sup>. This leads to longer spin injection length. As both effects are included in our theory, our calculation predicts that, when there is no applied electric field, the increase of the spin life time is more important with the introduction of impurities.

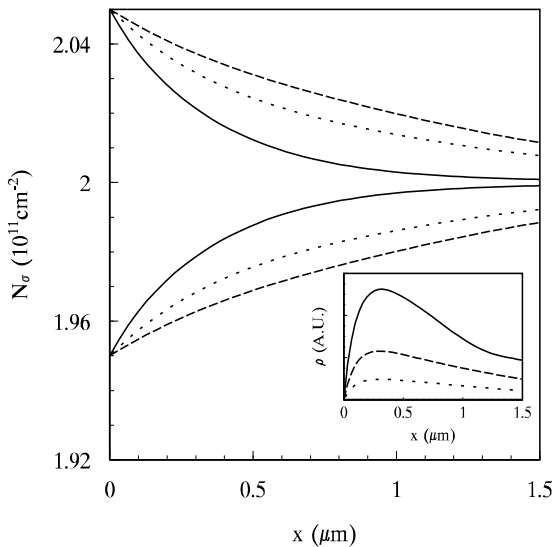


FIG. 5. Electron densities of up spin and down spin versus the position  $x$  for different temperatures. Solid curves:  $T = 120\text{K}$ ; Dotted curves:  $T = 200\text{K}$ ; Dashed curves:  $T = 300\text{K}$ . The corresponding spin coherences are plotted as function of the position  $x$  in the inset with the same curves as the electron densities.

In Fig. 5, we plot the the spin densities as functions of position  $x$  for the spin diffusion at three different temperatures  $T = 120, 200$  and  $300\text{ K}$ . The incoherently summed spin coherences are plotted in the inset. One can see from the figure that, contrary to the intuition, the decay of spin polarization decreases as the temperature increases and therefore one gets longer spin injection length for higher temperature. It is understood that

three effects influence the temperature dependence of the spin diffusion: The first is the electron diffusion constant, which decreases with the temperature. This results in faster decay of the spin signal with the increase of temperature. The second is the spin life time, which increases slightly with the temperature<sup>45</sup> (which can be justified by the the decay rate of the incoherently summed spin coherence at  $x > 1\text{ }\mu\text{m}$ ). This results in slower decay of the spin signal. The third one is the temperature dependence of the interference effect which originates from the temperature dependence of the electron distribution. From the simplified model in Sec. III, one can see that the electrons with small  $k_x$  contribute most importantly to the interference effect. As the temperature increases, there are more electrons distributing at the higher energy. Consequently, the distribution function of electron with small  $k_x$  decreases as the temperature increases. Therefore, the decay of spin signal due to interference effect decreases with the increasing of temperature. Our result indicates that decreasing of the decay of the spin signal due to the last two effects precedes the increasing of the decay of the spin signal that comes from the decreasing of the electron diffusion constant.

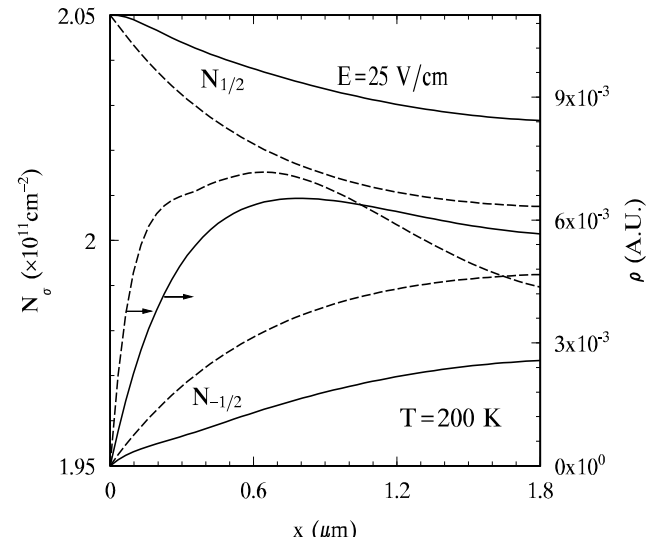


FIG. 6. Electron densities of up spin and down spin and the incoherently summed spin coherence versus the diffusion  $x$  for different applied electric field in intrinsic sample. Solid curves:  $N_\sigma$  and  $\rho$  for  $E = 25\text{V/cm}$ ; Dashed curves:  $N_\sigma$  and  $\rho$  for  $E = 0\text{V/cm}$ . Note the scale of the spin coherence is on the right side of the figure.

## B. $\mathbf{E} \neq 0$ case

We now turn to the spin transport in the presence of an applied electric field  $\mathbf{E} = E\hat{\mathbf{e}}_x$  along the diffusion direction. We first consider the case of the pure GaAs QW ( $N_i = 0$ ). In Fig. 6 the densities of the two spin bands are

plotted as functions of position  $x$  for the pure GaAs QW with the applied field  $E = 25$  V/cm. For comparison, we also plot the results with  $E = 0$  as dashed curves in the same figure. One can see from the figure that, with a finite applied electric field the spin signal decays much slower than that without electric field. For example, at  $x = 1$   $\mu\text{m}$  the decay of spin polarization is only about one half of that when the field is zero. Therefore in the presence of an applied electric field, the spin signal can transport much longer than the field-free case. This result is consistent with the significant current dependence of spin injection from Fe to GaAs<sup>43</sup>.

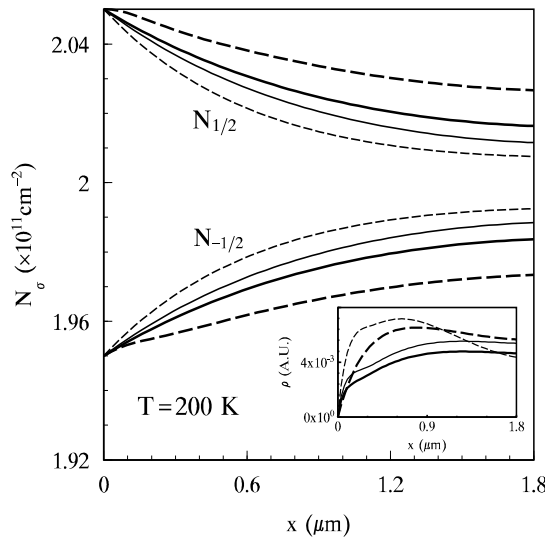


FIG. 7. Electron densities of up spin and down spin and the incoherently summed spin coherence versus the diffusion length  $x$  for different applied electric field and impurity levels. Thick solid curves:  $N_\sigma$  for  $E = 25$  V/cm and  $N_i = 0.4N_0$ ; Thin Solid curves:  $N_\sigma$  for  $E = 0$  and  $N_i = 0.4N_0$ ; Thick dashed curves:  $N_\sigma$  for  $E = 25$  V/cm and  $N_i = 0$ ; Thin dashed curves:  $N_\sigma$  for  $E = 0$  and  $N_i = 0.4N_0$ ; The corresponding incoherently summed spin coherences  $\rho$  vs.  $x$  are plotted in the inset with the same curves as those for electron densities.

This can be understood that in the presence of an applied electric field, electrons get a finite center-of-mass drift velocity  $\mathbf{v}_d = \mu\mathbf{E}$ , and move faster along the diffusion direction, provided the later is coincides with the direction of the electric field. This results in a smaller spatial decay of spin signal. It can be further justified by the slower decay rate of the incoherently summed spin coherences  $\rho$ , which are also plotted in Fig. 6. The same qualitative result is also achieved by using QIEM<sup>13–15</sup>.

It is interesting to note that impurities also decrease the electron mobility  $\mu$ . At the same applied electric field, the electron drift velocity of samples with impurities is smaller than that of pure samples. As shown above, the drift velocity affects the injection length effectively. Therefore in the presence of an applied electric field, the

impurities may *decrease* the spin injection length.

In Fig. 7 the electron densities of spin-up and -down bands are plotted versus the diffusion position  $x$ . The solid curves are for the data with impurities. For comparison, we also plot the results without impurities as dashed curves. The bold curves are for the results with  $E = 25$  V/cm and the thin curves are for the field-free results. It is seen from the figure that in the presence of impurities, by applying an electric field, one gets longer spin diffusion length (from the thin solid curve to the bold solid one). This is in the same trend as the impurity-free case (from this dashed curves to the bold dashed ones). However, in the presence of applied electric field, by adding impurities into the sample one gets smaller spin diffusion length. This is contrary to the field free case where impurities make the injection length longer.

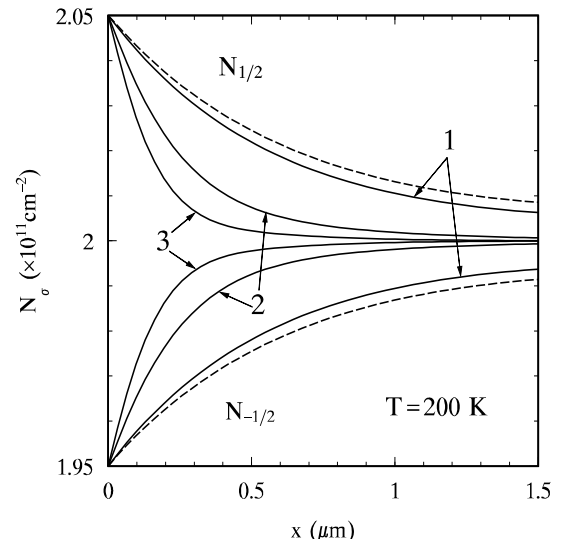


FIG. 8. Electron densities of up spin and down spin versus the diffusion length  $x$  for different interface electric field. Solid curve 1:  $E_z = 1 \times 10^3$  V/cm; Solid curve 2:  $E_z = 1 \times 10^5$  V/cm; Solid curve 3:  $E_z = 5 \times 10^5$  V/cm. Dashed curve:  $E_z = 0$ .

### C. Results with Rashba term

We now consider the interface electric field  $E_z$  dependence of the spin transport. As mentioned above, in GaAs QW the contribution of the Rashba term to the DP term is unimportant compared to that of the Dresselhaus term. Nevertheless, as the Rashba term is proportional to the interface electric field, it can be adjusted by applying an external bias electric field and therefore its effect can be demonstrated by applying a large field. We calculated the spin diffusion for three bias electric fields, which are  $10^3$ ,  $10^5$  and  $5 \times 10^5$  V/cm respectively. The results of electron densities for spin-up and -down bands are plotted against  $x$  for  $T = 200$  K as solid curves in Fig. 8. The electric field along the diffusion direction  $E$  is taken

to be zero. In the calculation, the spin-orbit constant  $\alpha_0$  is chosen to be  $5.33\text{\AA}^2$ <sup>44</sup>. Results with zero bias electric field is also plotted in the same figure as dashed curve for comparison. One can see from the figure that the decay of spin signal increases as the bias electric field increases. This is understood due to the stronger spin dephasing and decoherence introduced by the Rashba term.

#### D. Diffusion length

The QIEM predicates that the spin polarization decays exponentially along the diffusion direction according to

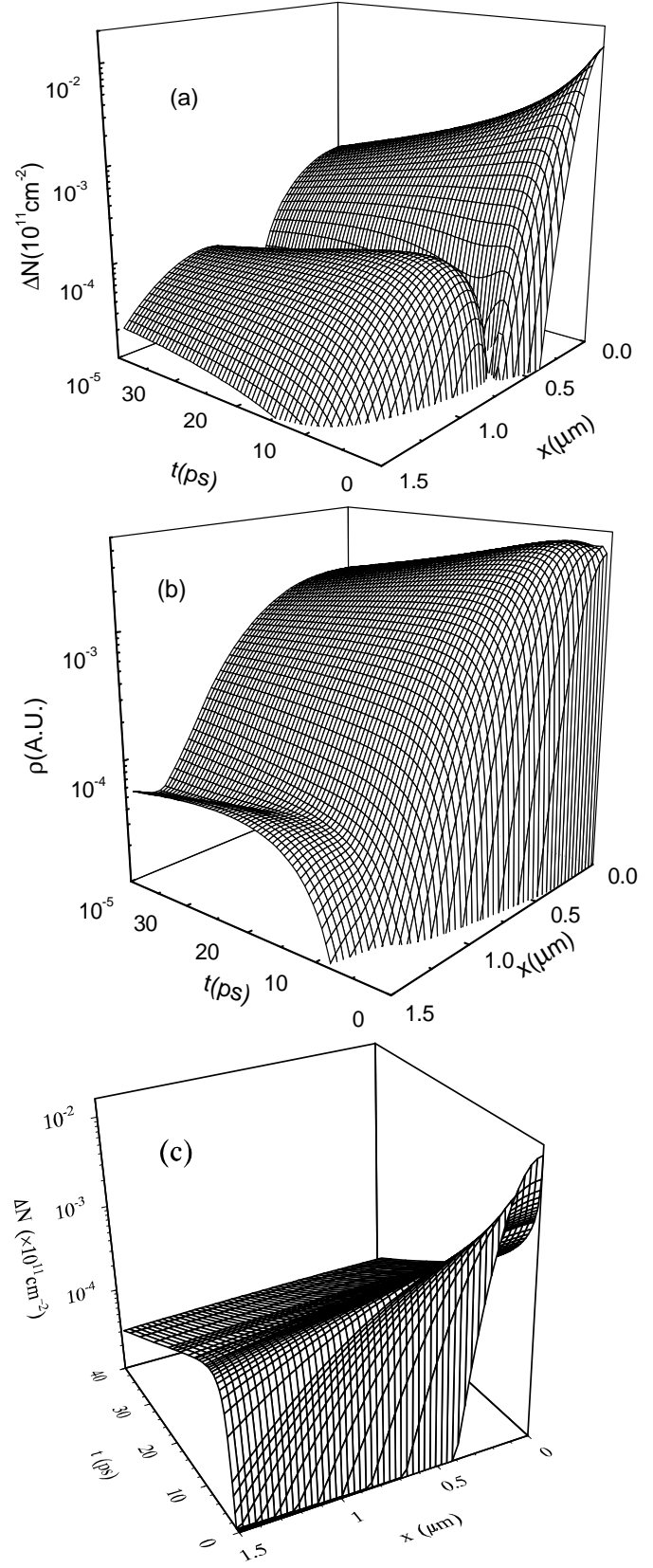
$$\Delta n(x) = \Delta n_0 e^{-x/L_s}. \quad (27)$$

$L_s$  is usually called the spin diffusion length or spin injection length. In QIEM, the injection length is defined as

$$L_s = \sqrt{D\tau_s}, \quad (28)$$

with  $\tau_s$  standing for the spin relaxation time and  $D$  representing the electron diffusion constant. The contribution to diffusion constant  $D$  comes from the scattering<sup>12,15</sup>. As we mentioned above that this simplified consideration throws away the interference effect of different  $\mathbf{k}$ 's. By fitting the spin polarization we get from our calculation as a function of the position  $x$  according to the form as Eq. (27), we can achieve the injection length which takes both the interference effect and the dephasing effect into consideration. By comparing the fitting injection lengths to the quasi-independent ones, we can get a rough estimation of the interference effect on the spin transport.

We list the injection lengths from our calculations in Table II. In this table, we also provide the injection length  $\sqrt{D\tau_s}$  predicated by the QIEM for comparison. In writing out the injection length of the QIEM, the electron diffusion constant is calculated by using the formula of Eq. (3) of Ref. 12, while the spin relaxation time  $\tau_s$  is calculated from Eq. (6) for the same QW under the spatial homogeneous condition<sup>45</sup> using the method discussed in detail in Refs. 19–21. The table shows that the diffusion lengths calculated through the full many-body equations are smaller than those predicated by the QIEM except the sample with impurities. Moreover, the decrease of the diffusion length with the interface electric field of our calculation is faster than that of QIEM. This justifies that the decoherence effect is more important at high (effective) magnetic field. One further notices from the table that the temperature dependence of the spin diffusion length predicated by these two model is different. The QIEM predicates that the diffusion length decreases as the temperature increases. However, by taking into account the temperature dependence of the interference effect, the spin diffusion length increases with the temperature in our full many-body theory.



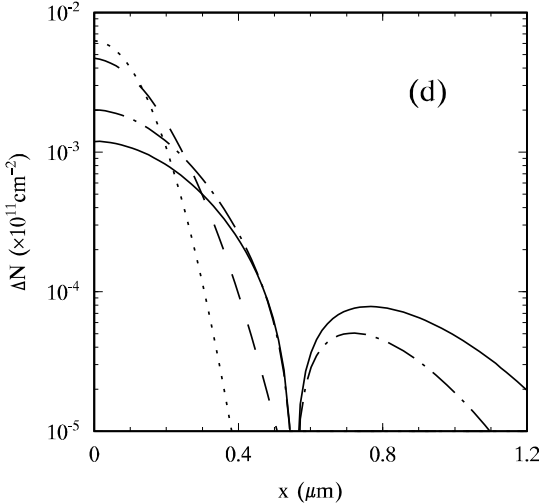


FIG. 9. (a). The difference of electron densities between the up spin and down spin versus the diffusion length  $x$  and time  $t$ ; (b) The incoherently summed spin coherence versus the diffusion length  $x$  and time  $t$ ; (c) The difference of electron densities between the up and down spin versus the diffusion length  $x$  and time  $t$  predicated by the QIEM; (d) The difference of electron densities between the up and down spin versus the diffusion length  $x$  at time  $t = 0$  (dotted curve),  $t = 1.1$  ps (dashed curve),  $t = 5.3$  ps (chained curve) and  $t = 10.7$  ps (solid curve).

## V. TRANSIENT DIFFUSION OF SPIN POLARIZATION

Above we have studied the spin diffusion/transport in the steady state. In fact, this many-body theory can also be used in studying time evolution of the spin polarized electron wave package (here and hereafter, we refer it as spin package). In this section, we assume a Gaussian-shaped spin package centered at  $x = 0$  at the initial time  $t = 0$  in an  $n$ -typed GaAs QW:  $\Delta N_{1/2}(x) = N_{1/2} - N_{-1/2} = \Delta N_0 e^{-x^2/\sigma^2}$  and compute the time evolution of this package when there is no applied electric field. The width of the package is  $\sigma = 0.15$   $\mu\text{m}$  and  $\Delta N_0 = 10^{10} \text{ cm}^{-2}$ . The initial spin coherence is assumed to be zero:  $\rho_{\sigma-\sigma}(x, \mathbf{k}, t = 0) = 0$ . The electron density of the QW is again assumed to be  $4 \times 10^{11} \text{ cm}^{-2}$ .

There are two processes of the time evolution of the spin package: The spin polarization of spin package decays with time due to the dephasing; In the mean time, it also diffuses due to the spatial inhomogeneity. In Figs. 9(a) and 9(b), we plot the difference between the electron densities of the two spin bands  $\Delta N = |N_{1/2} - N_{-1/2}|$  and the incoherently summed spin coherence versus time  $t$  and position  $x$ . As the spin package is symmetric to  $x = 0$ , we only plot the signal in the region of  $x \geq 0$ . For comparison, we also plot the result

predicated by the QIEM in Fig. 9(c).

It can be seen from the figures that, both full many-body kinetic theory and the QIEM predicate that the spin signals get a fast decay in the region of  $x < 0.12 \mu\text{m}$  due to the spin dephasing/decoherence as well as the diffusion. After 5 ps, the diffusion becomes less effective and the decay rates in these regime become smaller. For  $0.12 \mu\text{m} < x < 0.5 \mu\text{m}$ , the spin signals are first amplified by the diffusion from the regime  $x < 0.12 \mu\text{m}$  for  $t < 2$  ps. After 2 ps the spin polarizations in the regime of  $x < 0.12 \mu\text{m}$  has been reduced a lot and the diffusion to the regime of  $x > 0.12 \mu\text{m}$  becomes slower. Therefore one observes the decay of the spin polarization after 2 ps, which is the common effect of spin dephasing/decoherence and diffusion. For  $x > 0.5 \mu\text{m}$ , both models show that the spin signals can transport over  $1.5 \mu\text{m}$  away from the center after some time. Nevertheless, as the QIEM simplifies the problem by neglecting the spin correlation  $\rho_{\sigma-\sigma}$ , DP term and the Hartree-Fock term and treating the dephasing by relaxation time approximation, the details of the time evolution of spin package is quite different between these two models. For examples, our result shows that in the regime  $0.45 \mu\text{m} < x < 0.6 \mu\text{m}$ , for fixed  $x$  there are small oscillations of spin polarization with time. While these oscillations are absent in the results of the QIEM. These oscillations are due to the concurrent effect of the diffusion, dephasing and the spin flipping due the DP term.

The most striking difference between these two models is that, there exist oscillations of the spin polarization along the direction of diffusion from our many-body theory. In order to further elucidate this effect, we plot  $\Delta N$  against  $x$  at time  $t = 0, 1.1, 5.7$ , and  $10.3$  ps separately in Fig. 9(d). From this figure one can clearly see the spacial oscillation of the spin polarization when  $t > 3.5$  ps. This oscillation originates from the diffusion of the spin coherence  $\rho_{\sigma-\sigma}(x, \mathbf{k}, t)$  (with  $x < 0.55 \mu\text{m}$ ), which has been generated due to the spin precession (owing to the DP term) inside the spin package. Therefore, the spin coherence  $\rho_{\sigma-\sigma}$  at  $x > 0.55 \mu\text{m}$  gets excess. As the spin coherence sets up an effective local magnetic field, the excess field can change the spin polarization by flipping spin-up electrons to the spin-down ones and *vice versa*. Thus gives rise the oscillation in the spin diffusion. It is noted that in the QIEM, one only considers the longitudinal spin diffusion and therefore, there is no way to get the spin flipping from that theory.

## VI. CONCLUSION

In conclusion, we have performed a many-body investigation of the spin diffusion/transport in an  $n$ -doped GaAs QW based on a set of many-body kinetic transport equations. These equations are derived for the spatial inhomogeneous system by using nonequilibrium Green function method with generalized Kadanoff-Baym

Ansatz in a two-spin-band model<sup>20</sup>. It is noted that our theory takes all the inhomogeneous broadening effect, the spin diffusion due to the spacial inhomogeneity and the spin dephasing/decoherence into account and gets the results self-consistently.

We reexamine the wildly adopted QIEM and pointed out an important many-body spin decoherence effect which is missing in the single electron model. The new decoherence effect is based on interference effect of electrons/spins with different momentum  $\mathbf{k}$  along the diffusion direction, which is referred as “inhomogeneous broadening effect” in our paper. We have shown that this inhomogeneous broadening effect can cause the spin decoherence alone even without the scattering and that the resulting decoherence can be more important than the dephasing effect due to DP term together with the scattering part. Our study shows the inadequacy of the QIEM. Therefore, it is important to use the full many-body theory to study the spin transport.

We further study the spin diffusion/transport from the full many-body theory with the DP terms (The spin dephasing mechanism for  $n$ -typed GaAs QW at high temperature is the DP mechanism.) and the scattering included. By numerically solving the kinetic Bloch equations, together with the Poisson equation, we are able to investigate the spin diffusion in the steady state under the constant spin injection. We have shown the spin diffusion in the absence/presence of an applied electric field along the diffusion direction as well as with/without impurities. By applying an electric field along the diffusion direction, one gets much longer spin diffusion length as the electrons are driven by the electric field and get a net drift velocity. Also in the presence of the electric field, the spin diffusion length is reduced if one introduces impurities into the sample. However, when there is no applied electric field, the spin diffusion length is *enlarged* by adding impurities into the sample. This is contrary to what is predicted by the QIEM. The reason of this qualitative difference is also discussed. We also study the effects of the magnetic field in the Voigt configuration and the applied electric fields along the QW growth direction to the spin diffusion. In the present of the magnetic field, the spin polarization exhibits oscillation along the direction of diffusion and the decay due to the interference is much more effective than that of the dephasing and therefore the spin diffusion length is greatly reduced. We also investigate the spin diffusion at different temperatures. We find that as the temperature increases, the interference effect reduces as the electron distribution near  $k_x = 0$ , which is main contributor to the inhomogeneous broadening, becomes smaller. As a result, the spin diffusion length increases with the temperature. We show that the applied electric field along the growth direction makes the Rashba term more pronounced and hence both the decoherence and the dephasing get enlarged. Consequently the diffusion length is reduced.

We have also demonstrated the time evolution of the diffusion of a spin package. The spin signals near the

center of the package always decay with time due to the diffusion as well as the dephasing. Whereas the spin signals away from the center first increase then drop. For positions beyond the regime of the initial spin package, the spin polarization can be opposite to the initial one due to the spin flipping by the relatively large local effective magnetic field originated from the DP term together with the spin coherence  $\rho_{\sigma-\sigma}$ , with the later coming from both the diffusion and the spin precession. We also predict the spin oscillations with time at some positions. These features cannot be obtained from the QIEM. A thorough investigation about the time evolution of the spin package under different conditions is under way and the results will be published elsewhere.

## ACKNOWLEDGMENTS

MWW is supported by the “100 Person Project” of Chinese Academy of Sciences. He is also partially supported by Cooperative Excitation Project of ERATO (JST).

---

\* Corresponding author; Email: mwwu@ustc.edu.cn; Fax: +86-551-3601073; Tel: +86-551-3603524.

\*\* Mailing address.

<sup>1</sup> S.A. Wolf *et al.*, *Science* **294**, 1488 (2001).

<sup>2</sup> J.M. Kikkawa, I.P. Smorchkova, N. Samarth, and D.D. Awschalom, *Science* **277**, 1284 (1997).

<sup>3</sup> J.M. Kikkawa and D.D. Awschalom, *Nature* **397**, 139 (1999).

<sup>4</sup> J.M. Kikkawa and D.D. Awschalom, *Phys. Rev. Lett.* **80**, 4313 (1998).

<sup>5</sup> H. Ohno, *Science* **281**, 951 (1998).

<sup>6</sup> T. Adachi, Y. Ohno, F. Matsukura, and H. Ohno, *Physica E* **10**, 36 (2001).

<sup>7</sup> J.M. Kikkawa and D.D. Awschalom, *Science* **287**, 473 (2000).

<sup>8</sup> I. Malajovich *et al.*, *Phys. Rev. Lett.* **84**, 1015 (2000).

<sup>9</sup> B. T. Jonker, Y. D. Park, and B. R. Bennett, *Phys. Rev. B* **62**, 8180 (2000).

<sup>10</sup> G. Schmidt *et al.*, *Phys. Rev. B* **62**, R4790 (2000).

<sup>11</sup> M. Ziese and M. J. Thornton, *Spin Electronics*, (Springer, Berlin, 2001).

<sup>12</sup> M. E. Flatté and J. M. Byers, *Phys. Rev. Lett.* **84**, 4220 (2000).

<sup>13</sup> I. Žutić, J. Fabian, and S. Das Sarma, *Phys. Rev. B* **64**, 121201 (2001).

<sup>14</sup> Igor Žutić, Jaroslav Fabian, and S. Das Sarma, *Phys. Rev. Lett.* **88**, 066603 (2002).

<sup>15</sup> Z. G. Yu and M. E. Flatté, cond-mat/0201425.

<sup>16</sup> Ivar Martin, cond-mat/0201481.

<sup>17</sup> Y. Takahashi, K. Shizume, and N. Masuhara, *Phys. Rev. B* **60**, 4856 (1999).

<sup>18</sup> M.E. Flatte, J. Bayers, and W.H. Lau, unpublished.

<sup>19</sup> M.W. Wu and H. Metiu, Phys. Rev. B **61**, 2945 (2000).

<sup>20</sup> M.W. Wu, J. Supercond.: Incorporating Noval Mechanism **14**, 245 (2001); cond-mat/0109258; J. Phys. Soc. Jpn. **70**, 2195 (2001); M.W. Wu and M. Kuwata-Gonokami, Solid State Commun. **121**, 509 (2002).

<sup>21</sup> M.W. Wu and C.Z. Ning, Phys. Stat. Sol. (b) **222**, 523 (2000).

<sup>22</sup> M.I. D'yakonov and V.I. Perel', Zh. Eksp. Teor. Fiz. **60**, 1954 (1971) [Sov. Phys. JETP **38**, 1053 (1971)].

<sup>23</sup> G. Dresselhaus, Phys. Rev. **100**, 580 (1955).

<sup>24</sup> Yu. A. Bychkov and E.I. Rashba, J. Phys. C **17**, 6039 (1984).

<sup>25</sup> Yu A. Bychkov and E.I. Rashba, Sov. Phys. JETP Lett. **39**, 78 (1984).

<sup>26</sup> R. Eppenga and M.F.H. Schuurmans, Phys. Rev. B **37**, 10923 (1988).

<sup>27</sup> E.L. Ivchenko and G.E. Pikus, *Superlattices and Other Heterostructures*, (Springer, Berlin, 1995).

<sup>28</sup> A.G. Aronov, G.E. Pikus, and A.N. Titkov, Zh. Eksp. Teor. Fiz. **84**, 1170 (1983) [Sov. Phys. JETP **57**, 680 (1983)].

<sup>29</sup> G. Lommer, F. Malcher, and U. Rössler, Phys. Rev. Lett. **60**, 728 (1988).

<sup>30</sup> H. Haug and A.P. Jauho, *Quantum Kinetics in Transport and Optics of Semiconductors* (Springer, Berlin, 1996).

<sup>31</sup> J. Rammer and H. Smith, Rev. Mod. Phys. **57**, 323 (1986).

<sup>32</sup> T. Kuhn and F. Rossi, Phys. Rev. Lett. **69**, 977 (1992).

<sup>33</sup> X. D. Hu, R. de Sousa, and S. Das Sarma, cond-mat/0108339

<sup>34</sup> B. H. Floyd and Y. L. Le Coz, J. Appl. Phys. **76**, 7889 (1996).

<sup>35</sup> Y. L. Le Coz, Ph.D thesis, Massachusetts Institute of Technology, 1988.

<sup>36</sup> I. D'Amico and G. Vignale, Phys. Rev. B **65**, 085109 (2002).

<sup>37</sup> *Numerical Data and Functional Relationships in Science and Technology*, edited by O. Madelung, M. Schultz, and H. Weiss, Landolt-Börnstein, New Series, Vol. 17 (Springer Verlag, Berlin 1982).

<sup>38</sup> E.M. Conwell, *Solid State Physics*, suppl. 9, (Academic Press, New York, 1967).

<sup>39</sup> X.L. Lei and N.J.M. Horing, Int. J. Mod. Phys. B, **6**, 805 (1992).

<sup>40</sup> C.M. Hu *et al.*, Phys. Rev. B **63**, 125333 (2001).

<sup>41</sup> A. Fert, J.-L. Duvail, and T. Valet, Phys. Rev. B **52**, 6513 (1995).

<sup>42</sup> F. Meier and B.P. Zakharchenya, *Optical Orientation*, North-Holland Physics Publishing, Netherlands, 1984.

<sup>43</sup> A.T. Hanbichi *et al.*, Appl. Phys. Lett **80**, 1240 (2002).

<sup>44</sup> N.S. Averkiev, L.E. Golub, and M. Willander, J. Phys.: Cond. Mat. **14**, R271 (2002); Semiconductors **36**, 91 (2002).

<sup>45</sup> M.Q. Weng, T. Rao, M.W. Wu, and M. Ning, to be published.

$\kappa_0$	10.8	$\kappa_\infty$	12.9
$\Omega_{\text{LO}}$	35.4 meV	$m^*$	0.067 $m_0$
$g$	0.44	$E_g$	1.55 eV
$\alpha_0$	5.33 Å		

TABLE I. Parameters used in the numerical calculations

Curves	$L_s$ (μm)	D	$\tau_s$ (ps)	$\sqrt{D\tau_s}$ (μm)
Fig. 2, solid curve	0.7	0.114	16.0	1.35
Fig. 3, solid curve	1.0	0.022	23.4	0.72
Fig. 5, dashed curve 1	0.8	0.088	20.0	1.32
Fig. 5, solid curve 3	0.4	0.25	9.0	1.5
Fig. 8, solid curve 1	0.61	0.114	15.6	1.33
Fig. 8, solid curve 2	0.26	0.114	12.0	1.17
Fig. 8, solid curve 3	0.15	0.114	4.0	0.68

TABLE II. Spin injection length